Mechanically robust wrinkled liquid marbles

Mizuki TENJIMBAYASHI (天神林 瑞樹)[a)]

AFFLIATIONS

Research Center for Materials Nanoarchitectonics (MANA), National Institute for Materials Science (NIMS)1-1 Namiki, Tsukuba, Ibaraki 305-0044, Japan.

[a)]Author to whom correspondence should be addressed: TENJIMBAYASHI.Mizuki@nims.go.jp

Abstract

Liquid marble (LM) is a droplet covered with jammed low-wettability fine particles, which exhibits non-sticking to contacting media while keeping its fluid reconfigurability. While the LM facilitated the handling of the droplet, LM breaks down upon squeezing, which limits the robust handling. Here, we show that LM exhibits high compression stability when the jammed particles distort the liquid surface to form sub- to single-micron roughness. We find that the particle layers' distortion increases with the evaporation of the inner liquid. Thus, we regulated the evaporation degree of the droplet by varying the mixing ratio of the non-volatile and volatile liquids. First, we show the regulation of the mixing ratio and its effect on the equilibrium LM static shape and particle layer structure. Then, the effect of the LMs' surface structure on their mechanical response is explored. When 90% of the inner liquid is evaporated, the submicron wrinkle structure appears on the LM surface. We name the LM with the wrinkle structure "wrinkled liquid marble (WLM)." The WLM exhibited high compression stability and significantly higher resilience force than the droplet one. We believe this work helps the practical use of the LMs by improving their mechanical stability. Moreover, the fundamental understanding of the particle layer stability at the interface can be advanced.

Main

When the droplet is in contact with a low-wettable particle whose size is much smaller than the droplet, the droplet adsorbs the particles on its surface rather than dispersing inside. The droplets covered with the particle layer, known as liquid marbles (LMs),[1] roll-off/float-on the solid/liquid surfaces without sticking. Unlike the droplet covered with continuous solid, LMs exhibit shape reconfigurability, including split and coalescence.[2] Thus, LMs are an attractive carrier for delivering or releasing small amounts of liquid substances.[3,4] For example, the variation of the liquid substances allowed the LM to apply for chemical reactors,[5,6] detectors,[7] cell culturing platforms,[8–10] and healing agents.[11] For these applications, the stability of LMs[4], such as mechanical durabilitu[12] is essential.

Previously, the stability of the LM, the effect of the LMs parameter on their lifetime,[13–15] floating stability,[16,17] and mechanical durability were studied.[13,18] The studies focusing on mechanical durability include the effect of the particle size,[19,20] shape,[21] unjamming,[11] effective surface tension,[22] and/or substrate wettability[23] on the LM's compression or impact stabilities. While most works investigate the stability of the specific LMs, Liu et al.[20] or Asaumi et al.[19] report that the larger the microparticles, the higher mechanical compression stability the LM exhibits. Moreover, the micrometer-sized LMs are found to exhibit higher compression stability than the millimetric ones.[8] Other strategies to improve the mechanical stability are modifying the LM's contacting substrate[23] or introducing the viscous dissipation moiety to the particle layer.[24] Despite these efforts, the LM stability is still insufficient for robust mechanical transportation, such as picking up. Thus, the challenge is to suggest another strategy to improve mechanical stability further in a generally applicable manner.

In this work, we show that liquid surface structure formed by jamming of the particle layer contributes to improve the mechanical compression stability of the LM. Despite some works observing the jamming effect of the particle layer on the liquid surface structure,[25–30] their effect on the compression stability has not been clarified. Especially when the particle is highly condensed on the liquid surface, the wrinkle structure by the jammed particle layer is observed, as shown in **Fig. 1a**. This wrinkled LM (WLM) does not break down even under 90% compression (**Fig. 1b**). We expect the tolerance to the compressive deformation is owing to the wrinkle structure. Generally, spherical objects increase their surface area with deformation degree. Similarly, when classical LMs are deformed, particle density on the liquid surface decreases owing to the relative increase in the liquid surface area.[8] When the particle density is low enough to penetrate the inner liquid, the liquid penetration resisting pressure outweighs hydrostatic pressure, and LMs break down.[12] Thus, the wrinkled particle layer is expected to be tolerant to the deformation-induced decrease in particle density. Although this is not an example of LM, the wrinkled structure is known to be durable under deformable conditions.[31,32]

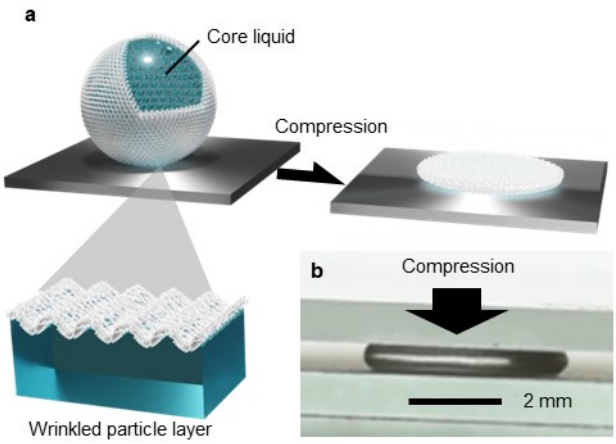

FIG. 1. (a) Illustration of a wrinkled liquid marble (WLM) exhibits the compression stability. See Figure 3b for the wrinkle structure. (b) No breakage of the WLM under ~90% compressed condition.

Figure 2 explains the method to control the particle number density on the LM surface. We formed LMs whose core liquid is the mixture of the non-volatile ionic liquid (IL) 1-(2-Hydroxyethyl)-3-methylimidazolium tetrafluoroborate and volatile ultrapure water (W). This work controls the mixture ratio IL_xW_{1-x} quantified with IL fraction x. We used the HMDS (hexamethyldisilazane)-treated hydrophobic fumed silica nanoparticles (AEROSIL® 300 (Evonik Industries, Germany)) with a primary diameter of ≈ 7 nm and aggregates of ≈ 100 to 200 nm (**Fig. S1**). Despite the slight decrease in the mixture surface tension with x, the contact angle on the HMDS-treated surface[33] was ≈ 80° in constant (**Fig. S2**). We formed the LM by gently rolling the mixture droplet on the nanoparticle-coated container with reference to Li's method.[27] The particles are adsorbed on the liquid surface with a random closed packing state from LM. We define the liquid volume and particle number density (unable to quantify because of the non-spherical fumed silica structure) just after the formation of the LM with V_0 and ψ_0, respectively (**Fig. 2a**). At this initial state, the particle number density does not depend on the mixture ratio x. However, when the LM is placed in ambient conditions (Temperature: 20 to 21°C, Humidity: 49 to 53%RH in this work), the volume of the volatile liquid is decreased or increased via water evaporation or adsorption from the air. Whether the volume increases or decreases depends on the x (**Fig. 2b**). After 24 hours, the droplet volume achieves the equilibrium, denoting the final state. We define the liquid volume and particle number density at the final state with V and ψ, respectively. Assuming the droplet is ideally spherical, the surface area is proportional to $V^{2/3}$. Since the particle number covering the droplet is the same between the initial and final state, we obtain the particle number density at the final state to be $\psi = \psi_0(V/V_0)^{-2/3}$. Thus, the volume ratio indirectly controls the particle number density of the LM, which is linearly proportional to the mixture ratio $x \sim V/V_0$ (**Fig. 2c**). Thus, we obtain $\psi \sim x^{-2/3}$. Moreover, **Figure 2c** indicates that the equilibrium liquid mixture ratio is $x \approx 0.9$, which clarifies the boundary condition $\psi = \psi_0$ at $x = 0.9$. We finally obtain the relationship $\psi \approx \psi_0(x/0.9)^{-2/3}$. Moreover, our focus is the mechanics of the LM with jammed particle layer distorts the liquid surface $\psi \geq \psi_0$. Thus, the mixture ratio is varied within the $0 \leq x \leq 0.9$ range.

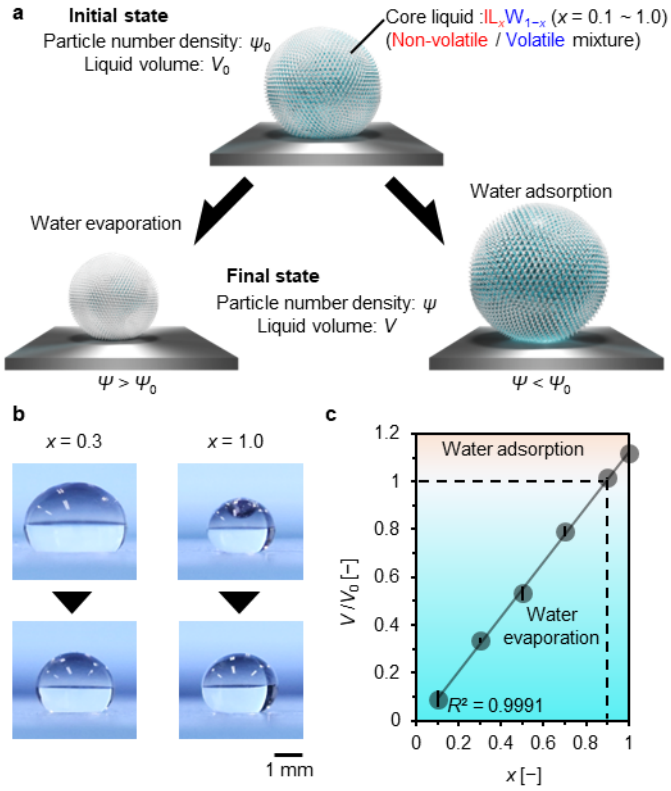

FIG. 2. (a) Method for controlling the particle number density of LMs. The non-volatile/volatile liquid mixture (ionic liquid IL_x/water W_{1-x}, where x is the mixture ratio) is used as core liquid (denote initial state). Depending on the mixture ratio, the droplet volume decreases/increases from V_0 to V (denote final state) via water evaporation/adsorption. The droplet volume change regulates the particle number density of the LM from ψ_0 to ψ. (b) Water evaporation or adsorption of the core liquid for x = 0.3 or 1.0. (c) Volume change of the core liquid V/V_0 as a function of x.

We obtained the LMs with the equilibrium volume of $V \approx 10$ μL from the different mixture ratio [NO_PRINTED_FORM]liquid by adjusting the initial liquid volume V_0. Note that the particle number density ψ increases with the decrease of x, and random close-packed LM (denoted as control) is the case for $x = 0.9$. **Figure 3a** shows photo images of the equilibrium LMs. We find optical variation in LMs with x. LM transitions from transparent to opaque in the visible range with the x decreases. Since the equilibrium core liquid composition does not differ with x, the optical change is due to the particle layer. **Figure 3b** shows their surface particle images obtained using differential interference contrast microscopy. For $x = 0.9$, we hardly observe the surface structure at the submicron scale, although concave-like domains are faintly observed. For $0.3 \leq x \leq 0.7$, the convex domains are observed on the LMs, possibly because the jammed particle layer deforms the liquid surface. We find the domain width increases from submicrometer to single micrometer with the decrease of x. This means that the distorted area of the liquid surface increases with the degree of evaporation. For $x = 0.1$, drastically different from others, the surface has high-density wrinkled patterns, and apparent light scattering by the pattern is observed. **Figure 3c** quantifies the surface roughness scale by observing the variation of color contrast as a function of line positions, which reveals that the wrinkle observed for $x = 0.1$ is highly periodic. The fitting by trigonometric function quantified the wrinkle wavelength to be ≈ 520 nm, which is comparable to the visible wavelength. Thus, the optical change in the LMs is due to the Mie scattering of the structured particle layer.[34] Here, we define the equilibrium LM for $x = 0.1$ with WLM. Notably, the observed wrinkle scale and uniformity differ from those formed by the particle thickness or liquid removing manner.[27,28,35] Generally, wrinkles are formed by buckling the thin, hard films on the soft substrate.[36] In this case, the film thickness, elasticity, and compression rate decide the wrinkle wavelength and the amplitude.[37] For WLM, the particle layer works as a solid film owing to the interfacial jamming transition despite the discontinuity.[38] The liquid layer works as the soft substrate because of its quasi-elasticity under non-sticking conditions.[39] The buckling force is expected to be the capillary force that works to minimize the surface area because the particle wettability hardly varied with the mixture ratio (**Fig. S2**); however, the jammed particles resist the surface minimization, resulting in buckling. Thus, the LMs sphericity quantified with h/d (h: LM height, d: LM width) slightly decreased with x decreases, as shown in **Fig. 3d**. We further observed the surface structure evolution by inner liquid evaporation in **Fig. 3e**, which also supports the water evaporation works to increase the surface roughness gradually.

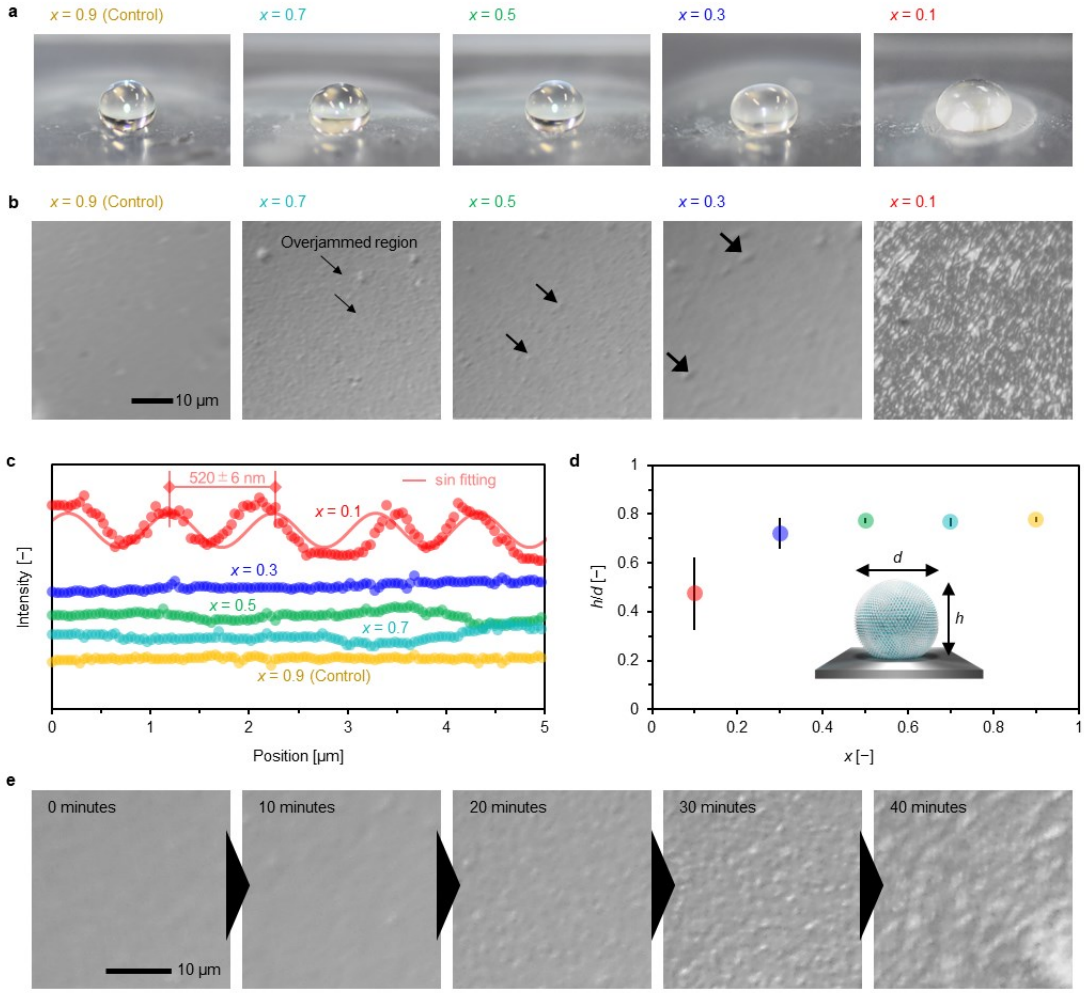

FIG. 3. Structural analysis of the LMs. (a) Photo images and (b) surface microscopic images of final state LMs ($V \approx 10$ μL) with different x. For $x = 0.9$, the droplet volume is not changed with time $V/V_0 = 1$. Thus, we regard the LM for $x = 0.9$ as the control LM. The LM for $x = 0.1$ has a wrinkled structure of the particle on the droplet surface, that is, WLM. The black arrow points to the convex domains on the LM surfaces. (c) Surface roughness profile of the LM with different x. For $x = 0.1$, we observed the periodic wavy structure whose wavelength is obtained by sin fitting. (d) LM sphericity quantified with h/d (h: LM height, d: LM width) variation with x. (e) DIC image of the surface structure evolution by water evaporation for $x = 0.1$. 0 minutes means the initial state. The observation light accelerates the evaporation.

Finally, we studied the compression resistance of the LMs with different x (**Fig. 4**). In the experimental setup, the LMs are sandwiched by two glass substrates, and the plate distance is gradually decreased at the speed of 0.1 mm/s. In compression, the resilience force of the LMs is monitored by microbalance. **Fig. 4a** shows the critical breakage height of the LMs. It is apparent that a significantly higher compression is required to break the LMs (x = 0.1 ~ 0.7) than the control one (x = 0.9). In particular, the WLM exhibited outstandingly high compression tolerance. **Fig. 4b** quantifies the resilience force f as a function of the compression rate $\sigma = z/h$ (z: compression length). Due to the control limit in particle coverage (mainly occurred by random close packing behavior of the particles at the initial state), there is fluctuation in the force curve even for the same x. Thus, we repeated the compression test at least 6 times, plotting all the force curves in the same graph. All the force curves are similar in shape in that the f grows accelerated with σ and suddenly decreases. The sudden decrease in the f means the breakage of the LMs. From the double-logarithmic graphs of the force curve, we find that all LMs obey the power law $f \sim \sigma^{3/2}$. The power law explains that the LMs can be regarded as the elastic sphere, known as the Hertz model.[40]

Figure 4c plots the critical resilience force f_c and compression rate σ_c just before the breakage. It is clear that the critical resilience force and the critical compression rate increased in the order of the LM for x = 0.1 >> 0.5 > 0.3 > 0.7 ≈ 0.9. It is apparent that the wrinkle formation effectively improves mechanical stability. Despite the expectation that the mechanical stability increased with x decreases, those for x = 0.3 and 0.7 are lower than expected. Let us check the roughness profile of the particle layer again (**Fig. 3b** and **3c**). We find that both LMs for x = 0.3 and 0.7 have "localized" micrometer-scale convex undulations, which may localize the compression stress to exhibit lower mechanical stability than expected. While this, LMs for x = 0.1 and 0.5 have uniformly distributed wrinkles/microdomains. Thus, as long as the LM has uniform surface roughness, liquid surface distortion by jamming of the particle layer drastically improves mechanical stability. We further discuss the particle layer effect (**Fig. 4c**-**4e**). If the LM elasticity solely corresponds to the liquid surface tension, we obtain the power law $f_c \sim \sigma_c^{3/2}$; however, we find the power law $f_c \sim \sigma_c^{3.7}$ from the double-logarithmic graphs of the critical resilience force and compression rate. This means that the particle layer effect contributes to increasing the elasticity. We expect the force chain contributing to the elasticity to be formed at the LM surface when the jammed particle layer distorts the liquid surface (**Fig. 4d** and **4e**). Under compression, the force chain may be composed of the particle elasticity by interparticle friction/pressure and liquid quasi-elasticity by localized Laplace pressure at the distorted liquid surface (**Fig. 4d**). These two elastic forces are alternatively connected at the WLM surface to form force the chain such as the series connection of the spring with different spring constant (**Fig. 4e**). In this model, inter-particle elasticity depends on the Young modulus of the particle and the particle surface roughness, and the liquid quasi-elasticity depends on the liquid surface tension and curvature of the distorted liquid surface.

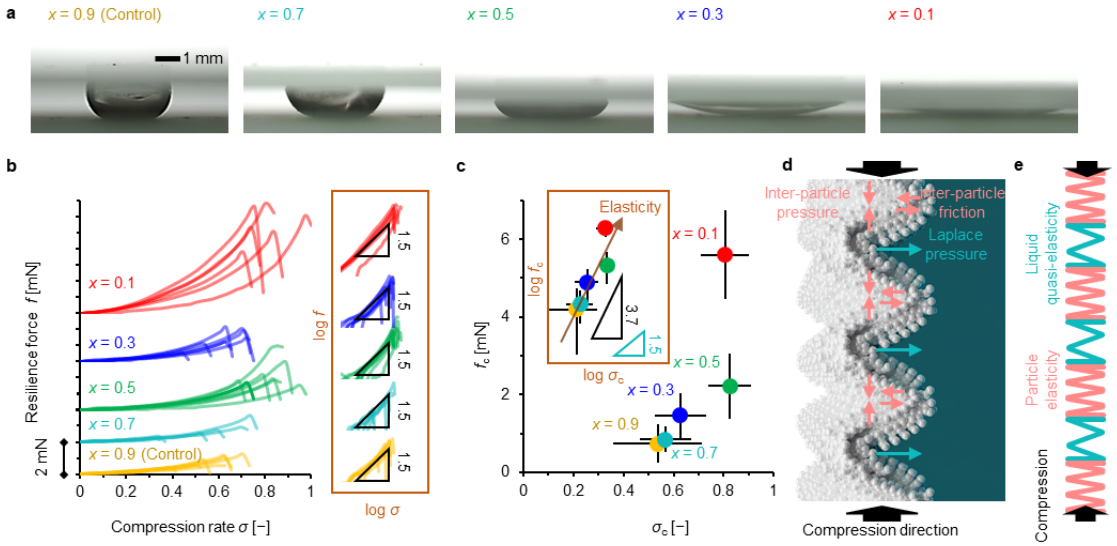

FIG. 4. (a) Side view images of the LM with different x just after the breakage by compression. (b) Resilience force f curves of the compressing LMs, where compression rate $\sigma = z/h$ (z: compression length). Their resolutions are 0.01 mN for f and 0.001 for σ. Inset is their double-logarithmic graphs. (c) The critical resilience force f_c and compression rate σ_c just before the breakage. Inset is their double-logarithmic graphs. (d) Illustration of the possible mechanical interactions and (e) force chain formation at the WLM surface in compression (Light red arrow: interparticle elasticity; Light blue arrow: Laplace pressure induced liquid quasi-elasticity).

In conclusion, we explored the effect of the jammed particle layer structure on LMs' mechanical stability. Our findings are: (i) Jammed particle layer, formed by the fumed silica nanoparticles with a primary diameter of ≈ 7 nm and aggregates of ≈ 100 to 200 nm, distorts the water surface to create the submicrometer to single micrometer scale roughness on LMs; (ii) When 90% of the inner liquid is evaporated, the LM with submicron wrinkle structure (WLM) is formed; (iii) Compression stability increased with the packing density although the non-uniform undulation can localize the compression stress; (iv) The particle roughness improve not only the critical compression rate but also the resilience force owing to the interparticle mechanical interaction. Since wrinkle formation on the liquid surface is a universal phenomenon to various particles used for LMs, we believe it can be the versatile strategy to improve the LM stability for its practical use. Moreover, we expect that further regulation of the wrinkle structure, such as wavelength and amplitude, may contribute to the flexible modulation of the LM mechanical property.

SUPPLEMENTARY MATERIAL

See the supplementary material for the particle structure and the droplet wettability.

ACKNOWLEDGEMENT

The author thank Ms. Makiko Yabune for supporting this study. This work was supported by the World Premier International Research Center Initiative (WPI), MEXT, Japan. This work is financially supported by JST FOREST (JPMJFR223V), and partially by JSPS KAKENHI (21H01643 and 23K18567).

AUTHOR DECLARATIONS

The authors have no conflicts to disclose.

DATA AVAILABILITY

The data that support the findings of this study are available within the article.

REFERENCES

[1] P. Aussillous, and D. Quéré, "Liquid marbles," Nature **411**(6840), 924–927 (2001).

[2] M. Tenjimbayashi, T. Mouterde, P.K. Roy, and K. Uto, "Liquid marbles: review of recent progress in physical properties, formation techniques, and lab-in-a-marble applications in microreactors and biosensors," Nanoscale **15**(47), 18980–18998 (2023).

[3] S. Fujii, S.I. Yusa, and Y. Nakamura, "Stimuli-Responsive Liquid Marbles: Controlling Structure, Shape, Stability, and Motion," Adv Funct Mater **26**(40), 7206–7223 (2016).

[4] J. Saczek, X. Yao, V. Zivkovic, M. Mamlouk, D. Wang, S.S. Pramana, and S. Wang, "Long-Lived Liquid Marbles for Green Applications," Adv Funct Mater **31**(35), 1–22 (2021).

[5] E. Sato, M. Yuri, S. Fujii, T. Nishiyama, Y. Nakamura, and H. Horibe, "Liquid marbles as a micro-reactor for efficient radical alternating copolymerization of diene monomer and oxygen," Chemical Communications **51**(97), 17241–17244 (2015).

[6] Z. Xin, and T. Skrydstrup, "Liquid Marbles: A Promising and Versatile Platform for Miniaturized Chemical Reactions," Angewandte Chemie International Edition **58**(35), 11952–11954 (2019).

[7] J. Tian, T. Arbatan, X. Li, and W. Shen, "Liquid marble for gas sensing," Chemical Communications **46**(26), 4734 (2010).

[8] M. Tenjimbayashi, S. Yamamoto, and K. Uto, "Drycells: Cell-Suspension Micro Liquid Marbles for Single-Cell Picking," Advanced Materials **35**(30), (2023).

[9] R.K. Vadivelu, H. Kamble, A. Munaz, and N.T. Nguyen, "Liquid marble as bioreactor for engineering three-dimensional toroid tissues," Sci Rep **7**(1), 1–14 (2017).

[10] F. Sarvi, K. Jain, T. Arbatan, P.J. Verma, K. Hourigan, M.C. Thompson, W. Shen, and P.P.Y. Chan, "Cardiogenesis of Embryonic Stem Cells with Liquid Marble Micro-Bioreactor," Adv Healthc Mater **4**(1), 77–86 (2015).

[11] M. Tenjimbayashi, S. Samitsu, and M. Naito, "Simultaneous Detection and Repair of Wetting Defects in Superhydrophobic Coatings via Cassie–Wenzel Transitions of Liquid Marbles," Adv Funct Mater **29**(26), 1–8 (2019).

[12] M. Tenjimbayashi, and S. Fujii, "How Liquid Marbles Break Down: Direct Evidence for Two Breakage Scenarios," Small **17**(37), 1–7 (2021).

[13] C. Fullarton, T.C. Draper, N. Phillips, R. Mayne, B.P.J. De Lacy Costello, and A. Adamatzky, "Evaporation, Lifetime, and Robustness Studies of Liquid Marbles for Collision-Based Computing," Langmuir **34**(7), 2573–2580 (2018).

[14] A. Tosun, and H.Y. Erbil, "Evaporation rate of PTFE liquid marbles," Appl Surf Sci **256**(5), 1278–1283 (2009).

[15] M. Dandan, and H.Y. Erbil, "Evaporation Rate of Graphite Liquid Marbles: Comparison with Water Droplets," Langmuir **25**(14), 8362–8367 (2009).

[16] P. Singha, C.H. Ooi, N.K. Nguyen, K.R. Sreejith, J. Jin, and N.T. Nguyen, "Capillarity: revisiting

the fundamentals of liquid marbles," Microfluid Nanofluidics **24**(10), 1–15 (2020).
[17] U. Cengiz, and H.Y. Erbil, "The lifetime of floating liquid marbles: The influence of particle size and effective surface tension," Soft Matter **9**(37), 8980–8991 (2013).
[18] Y. Rane, E. Foster, M. Moradiafrapoli, and J.O. Marston, "Compressive deformation of liquid marbles," Powder Technol **338**(October), 7–16 (2018).
[19] Y. Asaumi, M. Rey, K. Oyama, N. Vogel, T. Hirai, Y. Nakamura, and S. Fujii, "Effect of Stabilizing Particle Size on the Structure and Properties of Liquid Marbles," Langmuir **36**(44), 13274–13284 (2020).
[20] Z. Liu, Y. Zhang, C. Chen, T. Yang, J. Wang, L. Guo, P. Liu, and T. Kong, "Larger Stabilizing Particles Make Stronger Liquid Marble," Small **15**(3), 1–5 (2019).
[21] S. Azizian, S. Fujii, M. Kasahara, H.J. Butt, and M. Kappl, "Effect of particle morphology on mechanical properties of liquid marbles," Advanced Powder Technology **30**(2), 330–335 (2019).
[22] E. Bormashenko, R. Pogreb, G. Whyman, A. Musin, Y. Bormashenko, and Z. Barkay, "Shape, Vibrations, and Effective Surface Tension of Water Marbles," Langmuir **25**(4), 1893–1896 (2009).
[23] M. Tenjimbayashi, Y. Watanabe, Y. Nakamura, and M. Naito, "Exceptional Robustness and Self-Reconfigurability of Liquid Marbles on Superhydrophobic Substrate," Adv Mater Interfaces **7**(11), 2000160 (2020).
[24] M. Tenjimbayashi, and R. Tamate, "Particulate gel liquid marbles," J Mater Chem A Mater **12**(27), 16343–16349 (2024).
[25] X. Li, Y. Wang, Y. Yang, S. Wang, D. Zang, and X. Geng, "Dynamic behavior of droplets under interfacial jamming of nanoparticles," Appl Phys Lett **113**(13), (2018).
[26] M. Tenjimbayashi, and M. Naito, "Bioinspired Multi-Transformability of Superhydrophobic Nano-Magnetite Swarm for Adaptive Object Transportation," Adv Funct Mater **32**(32), (2022).
[27] X. Li, Y. Wang, J. Huang, Y. Yang, R. Wang, X. Geng, and D. Zang, "Monolayer nanoparticle-covered liquid marbles derived from a sol-gel coating," Appl Phys Lett **111**(26), (2017).
[28] X. Li, X. Pang, H. Jiang, M. Duan, H. Liu, Z. Yang, Y. Xi, and T.P. Russell, "Open millifluidics based on powder-encased channels," Proceedings of the National Academy of Sciences **120**(28), 2017 (2023).
[29] J. Niu, W. Liu, J.X. Li, X. Pang, Y. Liu, C. Zhang, K. Yue, Y. Zhou, F. Xu, X. Li, and F. Li, "Machining water through laser cutting of nanoparticle-encased water pancakes," Nat Commun **14**(1), 3853 (2023).
[30] H. Liu, X. Pang, M. Duan, Z. Yang, T.P. Russell, and X. Li, "A Simple Route for Open Fluidic Devices with Particle Walls," Advanced Materials **2413862**, 1–12 (2024).
[31] W.K. Lee, W. Bin Jung, S.R. Nagel, and T.W. Odom, "Stretchable superhydrophobicity from monolithic, three-dimensional hierarchical wrinkles," Nano Lett **16**(6), 3774–3779 (2016).
[32] T. Wen, T. Ma, J. Qian, Z. Song, X. Jiang, and Y. Yao, "Phase-transition-induced dynamic surface

wrinkle pattern on gradient photo-crosslinking liquid crystal elastomer," Nature Communications **15**(1), (2024).

[33] S. V. Slavov, A.R. Sanger, and K.T. Chuang, "Mechanism of Silation of Silica with Hexamethyldisilazane," J Phys Chem B **104**(5), 983–989 (2000).

[34] S.E. Orchard, "Light Scattering by Spherical Particles: Radiation Pressure, Asymmetry Factor, and Extinction Cross Section," J Opt Soc Am **55**(9), 1190 (1965).

[35] A. Gallo, F. Tavares, R. Das, and H. Mishra, "How particle-particle and liquid-particle interactions govern the fate of evaporating liquid marbles," Soft Matter **17**(33), 7628–7644 (2021).

[36] S. Nikravesh, D. Ryu, and Y.L. Shen, "Surface Wrinkling versus Global Buckling Instabilities in Thin Film-Substrate Systems under Biaxial Loading: Direct 3D Numerical Simulations," Adv Theory Simul **5**(9), 1–13 (2022).

[37] R. Huang, C.M. Stafford, and B.D. Vogt, "Wrinkling of Ultrathin Polymer Films," MRS Proceedings **924**(June 2014), 0924-Z04-10 (2006).

[38] V. Trappe, V. Prasad, L. Cipelletti, P.N. Segre, and D.A. Weitz, "Jamming phase diagram for attractive particles," Nature **411**(6839), 772–775 (2001).

[39] S. Asare-Asher, J.N. Connor, and R. Sedev, "Elasticity of liquid marbles," J Colloid Interface Sci **449**, 341–346 (2015).

[40] H. Butt, K. Graf, and M. Kappl, "Physics and Chemistry of Interfaces," Physics and Chemistry of Interfaces (September 2003), 10–11 (2003).